Molecular-dynamics simulation of collisional energy transfer from vibrationally highly excited azulene in compressed CO 2

C. Heidelbach, I. I. Fedchenia, D. Schwarzer, and J. Schroeder

Citation: The Journal of Chemical Physics **108**, 10152 (1998); doi: 10.1063/1.476474
View online: http://dx.doi.org/10.1063/1.476474
View Table of Contents: http://scitation.aip.org/content/aip/journal/jcp/108/24?ver=pdfcov
Published by the AIP Publishing

Molecular-dynamics simulation of collisional energy transfer from vibrationally highly excited azulene in compressed CO_2

C. Heidelbach, I. I. Fedchenia, D. Schwarzer, and J. Schroeder
Max-Planck-Institut für Biophysikalische Chemie, Am Fassberg 11, D-37077 Göttingen, Germany

(Received 19 June 1997; accepted 16 March 1998)

Results from nonequilibrium molecular-dynamics simulations of collisional energy transfer from vibrationally highly excited azulene in compressed CO_2 are compared with experimental results from our laboratory obtained under comparable physical conditions. As observed in the experiment, the cooling rates show a purely monoexponential decay of the excess energy. The influence of the microscopic solvent shell structure on these processes is investigated using the full three-dimensional anisotropic CO_2 structure around azulene obtained from the simulation. The analysis shows that local heating effects of any kind do not play a role in our model system. Predictions of the pressure dependence of the energy transfer rates by the isolated binary collision model are compared with results from the simulations using two different definitions of the collision frequency in dense fluids. © *1998 American Institute of Physics.* [S0021-9606(98)50224-3]

I. INTRODUCTION

Studying the density dependence of unimolecular reaction dynamics in the transition range between gas phase and condensed fluid offers a unique possibility to disentangle the complex effects that solvent structure and dynamics impose on liquid phase chemical reactions. In particular, efficiencies and mechanisms of energy-transfer processes that control thermal activation of reactants and stabilization of intermediates and products may differ significantly between gas and liquid.[1–4] In this context the range of applicability of the isolated binary collision model (IBC) for energy transfer in gases and liquids has been discussed at length.[1–8] The validity of this approach has only been tested recently in systematic experiments involving collisional energy transfer from highly vibrationally excited azulene[2] and cycloheptatriene[9] covering a broad density range in a variety of polyatomic solvents, thus significantly extending earlier measurements in liquid solution[10–12] and supercritical and liquid xenon.[13]

Since experimental investigations offer only a restricted view on the processes of interest on a molecular level and quantum dynamic scattering calculations are still impossible for even moderate size polyatomic systems, most theoretical efforts in this field have focused on classical trajectory calculations.[14–17] In the gas phase, this classical approach is an indispensable tool, e.g., in the prediction of microscopic energy-transfer rate coefficients $k(E',E)$ and transition probabilities $P(E',E)$. In contrast, much less is known about the condensed phase,[18–21] especially when other than simple monoatomic solvents are involved.

In a recent detailed experimental analysis of the energy transfer of vibrationally highly excited azulene over a wide pressure range ($\sim 10^{-2}$–400 MPa) we examined the applicability of the IBC model at high densities.[3,4] We showed that the density dependence of the energy-transfer rate follows an IBC model which relates the collision frequency to the radial distribution function $g(r)$ of an attractive hard-sphere particle in a Lennard–Jones fluid. However, this model completely neglects the internal structure of solvent and solute and uses an artificial intermolecular potential, such that additional effects on the energy-transfer process, as, e.g., local heating of the immediate surrounding of azulene, are ignored. Therefore a detailed knowledge of the structure and dynamics of the solvent in the vicinity of a highly excited solute at different pressures is the basis for understanding energy transfer over the whole pressure range and justifying such simple *a priori* models. In the present work we want to discuss the experimental results for the case of azulene solvated in CO_2, focusing mainly on the structural properties of the CO_2–azulene mixture, with the help of molecular-dynamics calculations at two different pressures: 3.2 and 250 MPa.

The outline of the paper is as follows: after a brief description of intra- and intermolecular potentials and the setup of the computer experiment, we present a comparison between experimental and simulated energy-transfer rates. Turning to a description of energy transfer on the microscopic level we then discuss the pressure dependence of structural and dynamical properties of the binary solution focusing on the spatial solvent shell structure and investigating the possible role of local heating of the solvent shell. Consequently, we address the question of the applicability of the IBC model by using different methods to define a collision frequency in dense fluids and comparing the pressure dependences with that of the simulated energy-transfer rates.

II. METHODS

We use classical microcanonical NEV (constant particle number, total energy, and volume) molecular-dynamics simulations[22] treating both solute and solvent completely flexibly. In order to assess the sensitivity of the simulation results with respect to the potentials used, we studied two model systems.

(1) Model a: A simplified model with reduced intramolecular potentials of azulene and CO_2. For this model, the number of intramolecular parameters is minimized and all

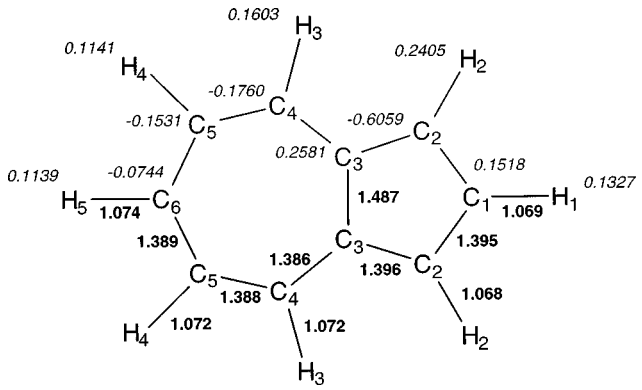

FIG. 1. C_{2v} structure of azulene. Italic numbers in the upper part assign atomic charges on the respective atoms. Bold numbers in the lower part give the respective bond lengths.

C–H stretch bonds which are not supposed to participate in the energy-transfer process are constrained with the SHAKE algorithm. For CO_2 the coupling term between the two stretching modes is omitted.

(2) Model b: Here the full intramolecular CO_2 potential is used together with an advanced intramolecular azulene potential which was tuned to reproduce experimental vibrational frequencies especially in the low-frequency domain of the azulene spectrum.

All intramolecular potentials are harmonic in internal coordinates except for those describing dihedral angles. The definition of the intramolecular azulene potential for model a is taken from Gebhardt[23] as a sum over bond stretch, bending, dihedral angle, and improper torsion contributions with the respective force constants k_r, k_θ, k_ϕ, and k_ω and equilibrium values r_0, θ_0, and ω_0 (cf. Fig. 1). The values of the force constants were taken from the QUANTA database[24] without modification (Tables I–IV):

$$\Phi_{\mathrm{azu}}=\sum k_r(r-r_0)^2+\sum k_\theta(\theta-\theta_0)^2 + \sum [|k_\phi|-k_\phi\cos(n\phi)]+\sum k_\omega(\omega-\omega_0)^2. \tag{1}$$

Nomenclature of atomic numbers and distances is given in Fig. 1. For model b the parameters were adjusted to reproduce the experimental vibrational frequencies. They are listed in Tables I–IV. Table V shows a comparison of the experimental frequencies with the results of normal-mode analyses of models a and b. As a measure for the quality of the simulated spectra we used the parameter χ which in our case, to avoid dominance of the high-frequency part of the spectrum, was defined as

$$\chi=\frac{1}{N}\sum_{\nu=1}^{N}\sqrt{\left(\frac{\Delta\tilde{\nu}_i}{\tilde{\nu}_i}\right)^2}, \quad N=48 \tag{2}$$

with $\Delta\tilde{\nu}_i$ being the difference between the simulated and the experimental frequency of mode i with experimental frequency $\tilde{\nu}_i$. We obtain χ values of 0.135 and 0.036, for

TABLE I. Force constants of the bend stretch potentials of azulene. Equilibrium bond lengths are given in Fig. 1.

Stretch: $a-b$	$U(r)=\Sigma k_r(r-r_0)^2$ k_r(kcal mol^{-1} Å^{-2})	
	Model a	Model b
C_1-C_2	450	400
C_2-C_3	450	400
C_3-C_3	450	400
C_3-C_4	450	300
C_4-C_5	450	300
C_5-C_6	450	300
C_1-H_1	380	360
C_2-H_2	380	360
C_4-H_3	380	360
C_5-H_4	380	360
C_6-H_5	380	360

TABLE II. Force constants and equilibrium angles for bend potentials of azulene.

Bend: $\sphericalangle a-b-c$	$U(\theta)=\Sigma k_\theta(\theta-\theta_0)^2$ k_θ(kcal mol^{-1})		θ_0 (deg)
	Model a	Model b	
$C_2-C_1-C_2$	65.0	80.0	109.824
$C_1-C_2-C_3$	65.0	80.0	108.516
$C_2-C_3-C_3$	65.0	60.0	106.572
$C_2-C_3-C_4$	65.0	43.3	126.159
$C_3-C_3-C_4$	65.0	43.3	127.268
$C_3-C_4-C_5$	65.0	80.0	129.151
$C_4-C_5-C_6$	65.0	80.0	128.555
$C_5-C_6-C_5$	65.0	80.0	130.047
$H_1-C_1-C_2$	23.0	32.0	125.088
$H_2-C_2-C_1$	23.0	35.0	126.199
$H_2-C_2-C_3$	-	35.0	126.286
$H_3-C_4-C_3$	23.0	37.0	115.274
$H_3-C_4-C_5$	-	37.0	115.575
$H_4-C_5-C_4$	23.0	33.0	115.751
$H_4-C_5-C_6$	-	33.0	115.694
$H_5-C_6-C_5$	23.0	30.0	114.977

TABLE III. Parameters for the dihedral angles of the intramolecular azulene potentials. The phase and periodicity are 180.0 and 2, respectively.

Dihedral angle: $\sphericalangle a-b-c-d$	$U(\phi)=\Sigma\|k_\phi\|-k_\phi\cos(n\phi)$ k_ϕ(kcal mol^{-1})	
	Model a	Model b
$C_1-C_2-C_3-C_4$	3.1	7.0
$C_2-C_1-C_2-C_3$	3.1	6.0
$C_2-C_3-C_4-C_5$	3.1	7.5
$C_2-C_3-C_3-C_4$	3.1	-
$C_3-C_3-C_2-C_1$	-	5.0
$C_3-C_3-C_4-C_5$	-	3.0
$C_4-C_3-C_3-C_4$	-	4.0
$C_5-C_6-C_5-C_4$	3.1	3.0
$C_6-C_5-C_4-C_3$	3.1	-
$H_1-C_1-C_2-C_3$	-	5.3
$H_2-C_2-C_1-C_2$	-	6.3
$H_2-C_2-C_3-C_4$	-	1.3
$H_3-C_4-C_3-C_2$	-	2.3
$H_3-C_4-C_5-C_6$	-	1.3
$H_4-C_5-C_4-C_3$	-	1.3
$H_4-C_5-C_4-C_3$	-	5.3
$H_5-C_6-C_5-C_4$	-	2.0

TABLE IV. Parameters for the improper torsions of the intramolecular azulene potentials. The phase and periodicity are 0.0 and 0, respectively.

Improper torsions: $\measuredangle a-b-c-d$	$U(\omega)=\Sigma k_\omega(\omega-\omega_0)^2$ k_ω(kcal mol^{-1})	
	Model a	Model b
$C_3-C_2-C_3-C_4$	90	-
$C_1-C_2-C_2-H_1$	75	30
$C_2-C_1-C_3-H_2$	75	30
$C_4-C_3-C_5-H_3$	75	30
$C_5-C_4-C_6-H_4$	75	30
$C_6-C_5-C_5-H_5$	75	30

model a and b, respectively, showing that the model b spectrum gives an entirely satisfactory match of the experimental frequencies.

In model b we use the intramolecular CO_2 potential published by Zhu and Robinson[25]

$$\Phi^{(a)}_{CO_2}=k_1((r_{12}-r_0)^2+(r_{13}-r_0)^2)+k_\theta(\theta-\theta_0)^2, \tag{3}$$

$$\Phi^{(b)}_{CO_2}=\Phi^{(a)}_{CO_2}+k_2(r_{12}-r_0)(r_{13}-r_0), \tag{4}$$

with

$k_1=1114.9$ kcal mol^{-1} Å^{-2},

$k_2=187.0$ kcal mol^{-1} Å^{-2} and $r_0=1.161$ Å,

$k_\theta=55.3$ kcal mol^{-1} and $\theta_0=\pi$.

Here r_{12} and r_{13} are the distances between the C atom and the oxygen atoms. In model a we omit the bond–bond interaction term of Eq. (4).

As discussed elsewhere,[26] among the different proposals for the CO_2–CO_2 intermolecular potential[27] we have chosen the functional form[28,29] which best reproduces the experimental data from neutron scattering in liquid carbon dioxide:

$$\Phi_{CO_2-CO_2}=\sum_i\sum_j\left[\exp\left(-\frac{r_{ij}-\sigma_{ij}}{\rho_{ij}}\right)+\frac{q_iq_j}{r_{ij}}-\frac{C^{(6)}_{ij}}{r^6_{ij}}F_{ij}(r_{ij})\right] \tag{5}$$

with

$$F_{ij}(r_{ij})=\begin{cases}\exp\left[-\left(\dfrac{1.28R^0_{ij}}{r_{ij}-1}\right)^2\right] & \text{if } \dfrac{1.28R^0_{ij}}{r_{ij}-1}>1\\ 1 \quad \text{elsewhere.}\end{cases} \tag{6}$$

With the original parameters given in Ref. 29 important solvent properties such as pressure, self-diffusion coefficients, and viscosity, were not reproduced for the conditions of interest.[26] Therefore the parameters were adjusted to reproduce the respective solvent self-diffusion coefficients at $p=3.2$ and 250 MPa (Table VI).

The azulene-CO_2 interaction was modeled by a combination of a 6-12 potential and Coulomb interaction:

$$\Phi_{azu-CO_2}=\sum_\alpha^{N_\alpha}\sum_\beta^{N_\beta}\left[\frac{q_\alpha q_\beta}{r_{\alpha\beta}}+\frac{A_{\alpha\beta}}{r^{12}_{\alpha\beta}}-\frac{B_{\alpha\beta}}{r^6_{\alpha\beta}}\right] \tag{7}$$

with α running over all 18 atoms of azulene and β over all atoms of CO_2 in the box. The parameters A and B, taken from the QUANTA database,[24] were treated as pressure independent. The respective values are $A_{CC}=468\,581.32$ kcal mol^{-1} Å^{12} and $B_{CC}=298.52$ kcal mol^{-1} Å^6 for the interaction of all C atoms in azulene with C atoms in carbon dioxide, $A_{CO}=241\,798.39$ kcal mol^{-1} Å^{12} and $B_{CO}=293.70$ kcal mol^{-1} Å^6 for the interaction of all C atoms in azulene with O atoms in carbon dioxide. For hydrogen atoms we used $A_{HC}=65\,638.44$ kcal mol^{-1} Å^{12} and $B_{HC}=103.71$ kcal mol^{-1} Å^6 and $A_{HO}=26\,503.84$ kcal mol^{-1} Å^{12} and $B_{HO}=90.84$ kcal mol^{-1} Å^6 for carbon dioxide C- and O-atom interactions, respectively. Azulene atomic charges were obtained by fitting them to a 6-311G** electron density under the constraint of a fixed experimental di-

TABLE V. Comparison of results from the normal-mode analysis of models a and b with experimental frequencies (Ref. 52) (in cm^{-1}). The normal-mode frequencies of model a deviate strongly from the experimental results, especially in the low-frequency part of the spectrum.

Mode:	$\tilde\nu_{exp}$	$\tilde\nu_a$	$\tilde\nu_b$	Mode:	$\tilde\nu_{exp}$	$\tilde\nu_a$	$\tilde\nu_b$	Mode:	$\tilde\nu_{exp}$	$\tilde\nu_a$	$\tilde\nu_b$
1	189	131	185	17	900	686	859	33	1378	1330	1398
2	240	132	238	18	911	702	866	34	1396	1374	1420
3	304	231	327	19	941	746	916	35	1443	1469	1480
4	323	259	330	20	952	772	948	36	1448	1480	1496
5	331	267	392	21	965	784	967	37	1457	1585	1528
6	406	340	395	22	971	837	967	38	1480	1644	1578
7	486	350	434	23	987	850	999	39	1536	1702	1598
8	542	418	545	24	1012	873	1016	40	1579	1767	1642
9	562	436	554	25	1049	888	1027	41	2968	3113	3028
10	680	574	582	26	1058	955	1029	42	3018	3113	3028
11	712	598	588	27	1117	1007	1041	43	3037	3113	3031
12	731	605	745	28	1160	1018	1067	44	3037	3115	3034
13	762	615	759	29	1210	1072	1130	45	3042	3116	3036
14	795	630	785	30	1216	1096	1174	46	3072	3116	3036
15	813	668	789	31	1268	1216	1224	47	3077	3117	3036
16	825	673	852	32	1300	1235	1296	48	3098	3120	3039

TABLE VI. Pressure-dependent parameters for the intermolecular CO_2–CO_2 potential [Eqs. (5) and (6)] in the simulations to reproduce diffusion coefficients and viscosity at the required pressures.

	q_i	ρ_i	σ_i	R_i^0	$C_{ii}^{(6)}$
		3.2 MPa			
C	0.280	0.253 29	0.854 72	41.93	2.65
O	−0.140	0.241 66	1.368 90	41.93	2.65
		250 MPa			
C	0.748	0.253 29	0.854 72	43.18	2.65
O	−0.374	0.241 66	1.368 90	43.18	2.65

pole moment of 0.8 D,[30,31] using the CHELPG algorithm within the GAMESS *ab initio* package[32] (Fig. 1).

For the simulation we used a cubic simulation box, containing one azulene and 216 CO_2 or 337 CO_2 molecules for the low- and high-pressure simulations, respectively. The corresponding box lengths are 72.78 and 27.027 Å, respectively. The time step of integration was chosen to be 0.5 fs. Short-range interactions were truncated at half the box length, whereas long-range electrostatic forces were treated with the Ewald summation technique. All simulations were performed with the CHARMM[33] package which was modified to our needs.

In the experimental setup azulene is excited with a laser to the S_1 state. After ~1 ps the molecule comes back to the ground electronic surface by internal conversion leading to a vibrationally highly excited species without equilibration of the surrounding medium. Therefore in order to simulate collisional energy transfer under comparable conditions all CO_2 atoms in the simulation box were held fixed while the azulene was heated up to 1100 K. After equilibration of azulene at this temperature for 5 ps, the constraints on carbon dioxide were dropped and the energy flow was sampled every 4 fs. After reaching equilibrium the simulation box was cooled down to its starting temperature at the respective pressure, equilibrated for 25 ps, and afterwards the procedure was repeated. The final decay curves were obtained by averaging 40 data sets at high pressure but only 20 data sets at low pressure, due to the length of the calculations.

The extent of equipartition of the energy in the ''hot'' azulene molecule was tested by the criterion

$$\langle \sqrt{m_i m_j} v_i v_j \rangle = kT \delta_{ij}, \tag{8}$$

where m_i and v_i represent mass and velocity of the ith atom of azulene. Since off-diagonal terms were usually in the range of ~1% of the diagonal terms we concluded that the starting energy distribution was very close to microcanonical.

To assess the influence of finite box size effects for model a at high pressure, the system with the shortest relaxation time, also simulations with a reduced number of 216 CO_2 molecules were performed. Within statistical error this simulation gave the same relaxation rates as that with 337 molecules.

For the investigation of structural properties, the trajectory was propagated at the equilibrium temperature for 1.05 ns, sampling configurations every 250 fs. For the evaluation of vibrational cooling rates and collision frequencies the sampling interval was decreased to 4 fs.

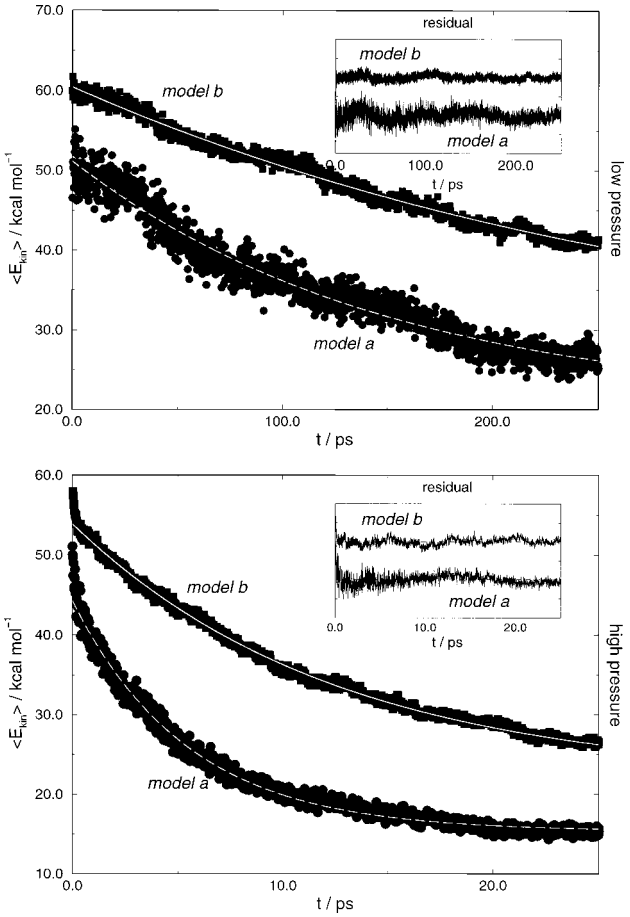

FIG. 2. Loss of kinetic energy from azulene as a function of time at 3.2 (top) and 250 MPa (bottom). The initial temperature of azulene is ~1100 K. The bath was equilibrated at 445 or 298 K at low and high pressure, respectively. The shaded functions correspond to the simulated values. The dashed and solid lines represent monoexponential fits with decay times of $\tau = 150.30$ or 5.43 ps for model a and $\tau = 306.32$ or 12.54 ps for model b at 3.2 and 250 MPa, respectively. The larger noise of the signals at low pressure is due to lower statistics. The insets show residuals of the monoexponential fits.

III. RESULTS AND DISCUSSION

A. Energy-transfer rates

We have calculated energy-transfer rates at 3.2 MPa and 445 K, where real CO_2 is in a supercritical state and at ~300 MPa and 298 K, where the liquid solvent is slightly below the critical isotherm. In agreement with the experiment, in all cases the decay of the total kinetic energy $E_{\mathrm{kin}} = \frac{1}{2}\Sigma_{i=1}^{18} m_i v_i^2$ of azulene is monoexponential (Fig. 2). For model a decay times amount to 150.3 and 5.4 ps for low and high pressure, respectively. With the change of potential to model b these relaxation times increase to 306.3 and 12.5 ps, respectively. Errors on the time constants were estimated to ~10%. Because of the length of the required trajectories only 20 trajectories have been calculated at low pressure for each model. Thus the larger noise of the decay curves at 3.2 MPa is due to worse statistics. Considering that the azulene–

TABLE VII. Decay time constants of the potential part of the azulene Hamiltonian at 250 MPa for model a. Within the error of the calculations all parts show monoexponential decay behavior at roughly the same rate, indicating that IVR is fast in comparison to the energy flow to the surrounding medium.

$\langle E \rangle$	τ/ps^{-1}
r	6.029 ± 0.035
θ	5.725 ± 0.070
ϕ	5.216 ± 0.014
ω	5.289 ± 0.064
Total	5.549 ± 0.035

CO_2 potential was not treated as pressure dependent in these calculations, these rates satisfactorily reproduce the pressure effect observed in experiment which gave 213 and 18.7 ps under comparable low- and high-pressure conditions, respectively.

For model b the decay times are by a factor of ~ 2 larger than the results from model a. This decrease of the energy-transfer rate as a function of the intramolecular azulene potential can be interpreted in terms of the azulene spectrum. For model b the low-frequency modes, which are supposed to contribute most to the energy flow into the medium, are higher in frequency by about 20%. Thus the coupling of azulene to the surrounding becomes weaker and the energy transfer is less efficient. However, two more points have to be noted in conjunction with the decay curves. First, in spite of starting at the same initial temperature, i.e., kinetic energy per degree of freedom, the initial energy of model a lies ~ 6 kcal mol^{-1} below model b. This is due to the use of the SHAKE algorithm to constrain the stretch of C–H bonds in model a, reducing the phase space of azulene by six degrees of freedom. Second, the residual plot (cf. inset of Fig. 2), i.e., the difference between the simulated data and the monoexponential fit, indicates a fast initial energy loss on a subpicosecond time scale at high pressure. At first sight, this process could be connected to local heating of the first solvation shell around azulene. According to our analysis (see below), however, this definitely is not the case. The fast component is rather due to a loss of azulene translational and rotational excess energy and is clearly an artifact resulting from our way of preparing the initial state of azulene which does not exclude these modes from being excited. In the process of equilibrating the vibrationally hot azulene at high pressure, the frozen CO_2 environment induces strong coupling between vibrational, rotational, and translational modes in azulene leading to a rotationally and translationally ''hot'' solute molecule. At low pressure, interaction with the surrounding CO_2 is much weaker, and azulene, in essence, behaves like an isolated molecule conserving its center-of-mass velocity and angular momentum ($\langle E_{\mathrm{com}} \rangle \approx \langle E_{\mathrm{rot}} \rangle \approx 1.4$ kcal mol^{-1} corresponding to $T \sim 450$ K). In this case, therefore, during the initial period of the nonequilibrium simulation the solute molecule is rotationally and translationally cold and no fast component of the cooling process appears in the results of the simulation.

As a manifestation of the equipartition principle, the po-

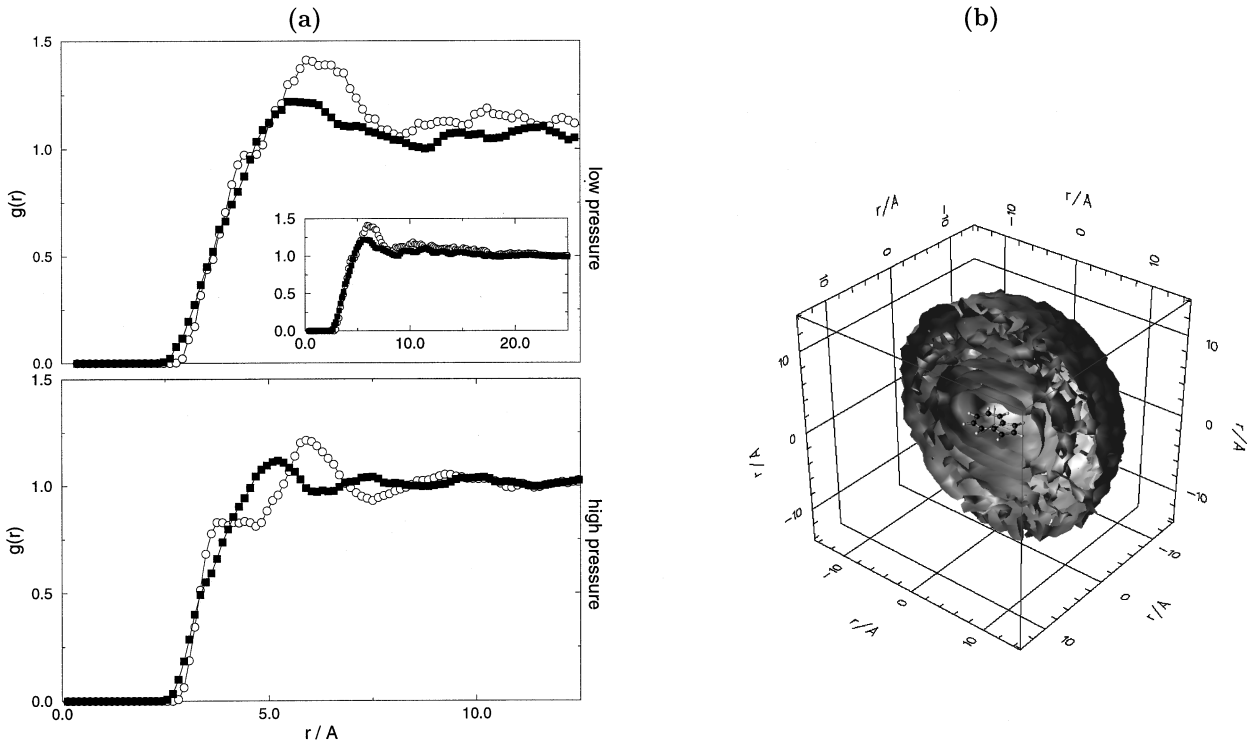

FIG. 3. Pair correlation functions (a) of CO_2 around the COM of azulene at 3.2 and 250 MPa. (○) distribution of C atoms, (■) distribution of O atoms in comparison to (b) an isosurface of the full spatial distribution of CO_2 molecules (30% maximum value) around azulene at 250 MPa. The sharp structure inherent in both pair distribution functions and the spatial distribution function at 250 MPa indicate a well-defined solvent structure with a high degree of anisotropy around the solute at this pressure.

a) probability : 1%

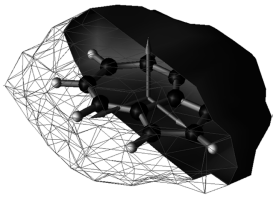

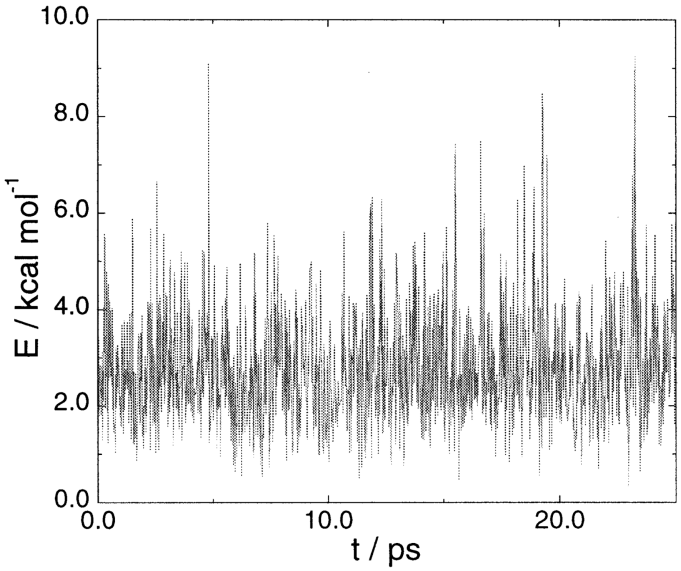

b) probability : 10%

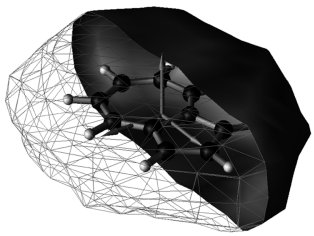

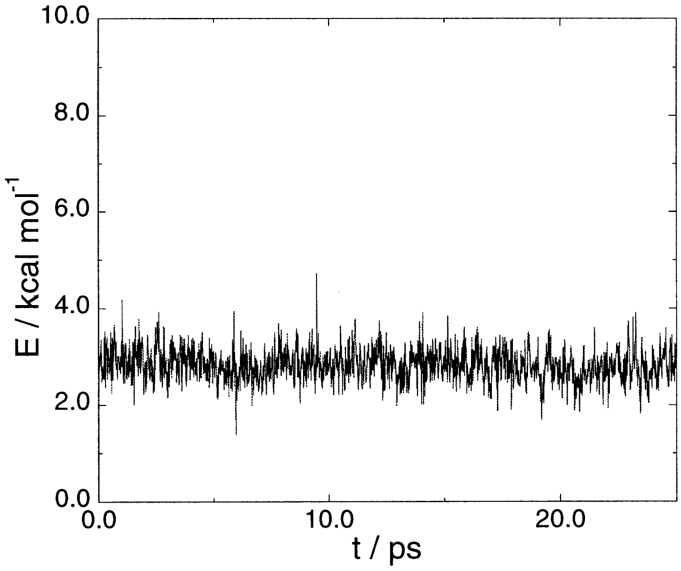

c) probability : 50%

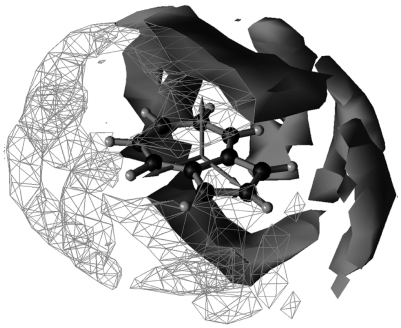

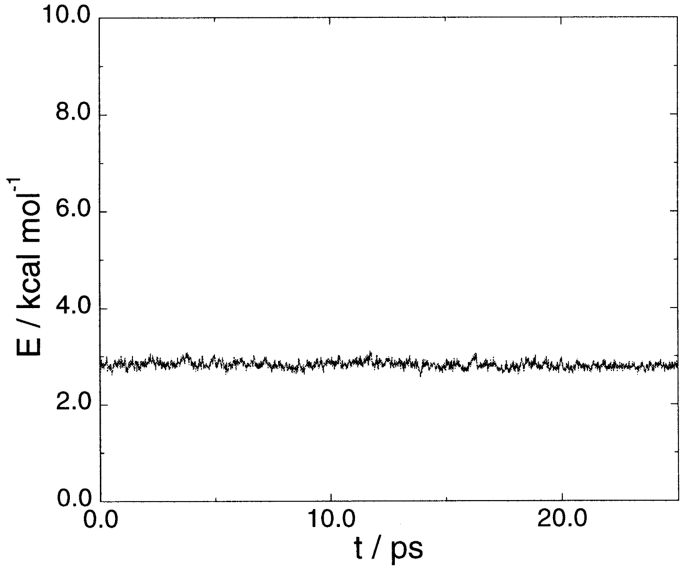

FIG. 4. Kinetic energy of CO_2 within the inner three solvation shells around azulene during energy transfer. Solvation shells correspond to isosurfaces of the full spatial distribution function of CO_2 around azulene at probabilities of 1%, 10%, or 50% of the maximum value for (a), (b), and (c), respectively. Within statistical error the mean kinetic energy of CO_2 molecules within these shells remain constant during the whole nonequilibrium simulation.

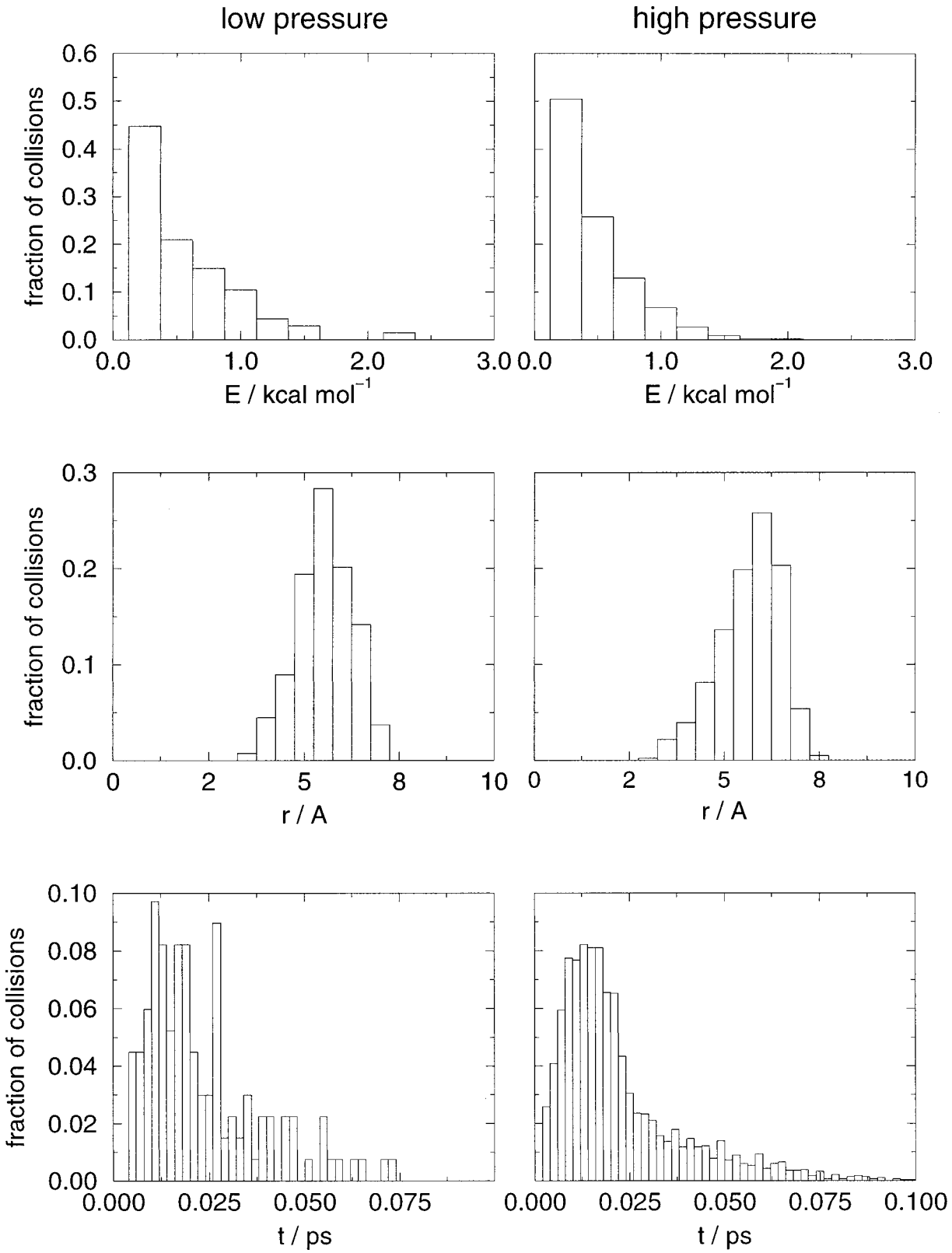

FIG. 5. Statistical data on collisions (energetic definition) for low (left column) and high pressure (right column). Characteristic properties for the collision process, namely the collision energy, radius, and time, are almost pressure independent.

tential energy of azulene in our calculations exhibits the same decay behavior as the kinetic part of the Hamiltonian (Table VII). Even at high pressure, all parts of the azulene intramolecular potential—bond stretches, bond angles, dihedral angles, and improper torsions—within statistical error lose their energy monoexponentially at the same rate, indicating that at least within this classical model intramolecular vibrational redistribution (IVR) is not a rate limiting factor for the overall process. This result is in agreement with experimental observations.[2] On the other hand, as stated by

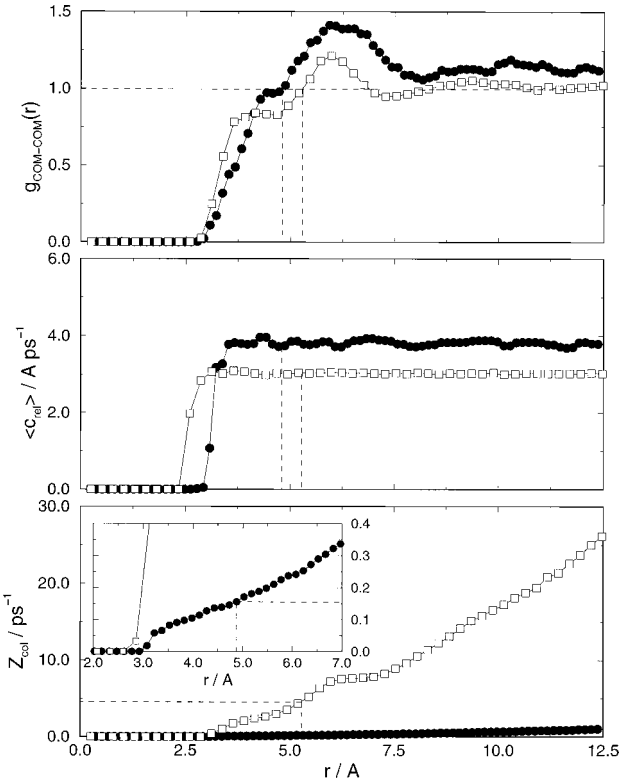

FIG. 6. Collision frequencies evaluated on the basis of the geometric definition by Oppenheim *et al.* (Ref. 36) at 3.2 (●) and 250 MPa (□). The frequencies are calculated at the marked distances, where the respective pair correlation function equals unity. For this calculation $g(r)$ at low pressure was smoothed with a five point spline (Ref. 22).

Nordholm and others,[34] since the solute molecule is large, 48 vibrational degrees of freedom, the actual energy per mode, even at 1100 K, is small. Therefore zero-order states are expected to be well separated and only weakly coupled to each other leading to a retardation of mode to mode energy transfer in a quantum picture. Thus classical molecular dynamics are bound to overestimate the IVR efficiency especially when, as in our case, no corrections for zero-point effects are taken into account.

B. Solvent shell structure

In 1971 Davis and Oppenheim for the first time proposed a connection between structural properties of a liquid and energy-transfer rates,[35,36] and there can be no doubt that the microscopic solvent structure in the vicinity of the solute has a certain impact on energy flow. This can be exemplified, as we have shown recently, by the density and temperature dependence of the collisional deactivation rate constants of highly excited azulene which is satisfactorily explained by local density influences on binary collision numbers.[3]

Molecular-dynamic simulations have been extensively used to explore structural properties of pure solvents[26,37,38] as well as of binary mixtures.[39–41] In our case, in order to investigate the pressure dependence of the solvent structure, radial distribution functions of the CO_2 molecules around the center of mass (COM) of azulene $g(r)_{\text{COM-C}}$ and $g(r)_{\text{COM-O}}$ were calculated at low and high pressure (Fig. 3). As the intermolecular potentials, i.e., the CO_2–CO_2 and CO_2–azulene interaction, remain unchanged, both model systems a and b exhibit the same structural properties. Thus we do not distinguish between the two models in the following discussion of structural influences.

For both thermodynamic states $g(r)$ has a similar form. The function drops to zero at about 2.6 Å, due to the strong repulsive force between solute and solvent at short distances. At 250 MPa the pair correlation functions reach their constant value at about 11 Å, where the solvent structure looses its correlation with the solute, whereas at 3.2 MPa, where the simulation box length is 73 Å, the complete decay lasts ~22 Å. At 250 MPa both $g(r)_{\text{COM-C}}$ and $g(r)_{\text{COM-O}}$ show various maxima in the region between 3 and 10 Å, corresponding to solvation shells around the central solute molecule. These well-defined structures of the pair correlation function are much less pronounced at low pressure. The peaks broaden, leading to single maxima at 5.3 and 5.8 Å for the oxygen and the carbon distribution, respectively. In addition to this, the plateau in $g(r)_{\text{COM-C}}$ which appears at high pressure at ~3.5 Å and indicates a high degree of anisotropy in the solvent structure at this pressure [cf. Fig. 3(a)], is not present at 3.2 MPa.

By definition $g(r)$, as a radial function, does not account for any angular dependence of the CO_2 distribution. To study this problem we have evaluated the total solute–solvent spatial distribution function and investigated orientational properties of carbon dioxide in the vicinity of azulene. To illustrate this complex four-dimensional distribution at 250 MPa, we use a visualization similar to that of Svischev and Kusalik,[42,43] which has proven valuable in the analysis of the structural and orientational properties of liquid CO_2.[26] Accordingly, in Fig. 3 and in the left column of Fig. 4 we show isosurfaces of the C-COM distribution obtained by cutting the full pair correlation function at a certain level of probability.

At 90% of the maximum probability, caps appear parallel to the azulene molecular plane at a distance of about 3.7 Å and almost perpendicular above the COM of azulene. These caps are equivalent to the first peak in $g(r)_{\text{COM-C}}$ [Fig. 3(a)]. By decreasing the probability, the initial caps broaden, shielding nearly the total solute in this direction. In addition to this, CO_2 molecules are now found in the molecular plane leading to a cagelike structure enclosing the azulene molecule at a probability 50% [Fig. 4(c)]. At a level of 30% of the maximum probability density the full cage structure is visible in the form of closed shells illustrating the anisotropy of the local liquid structure in the vicinity of azulene [Fig. 3(b)].

Moreover, various other shells appear, exhibiting lower amounts of anisotropy with increasing distance from the central molecule. At a final value of 1% of the maximum probability value these intermediate shells have vanished leaving only two shells intact, the collision shell, corresponding to the CO_2 molecules which collide with the highest kinetic energy [Fig. 4(a)], and the spherical bulk shell, reflecting the geometry of the simulation box (not shown here).

TABLE VIII. Calculated decay time constants τ for the total kinetic energy of azulene and experimental cooling times (Ref. 2) at thermodynamic states given. Simulated collision rates Z_{col} were calculated using the energetic definition (see text). Experimental collision rates are calculated from Lennard–Jones collision rates scaled by diffusion coefficients D (Ref. 2).

	Low pressure			High pressure		
	Model a	Model b	Exp.	Model a	Model b	Exp.
ρ/mol dm^{-3}	0.93	0.93	0.93	28.69	28.69	29
p/MPa	3.31	3.26	3.2	258.65	273.48	308.0
T/K	443.2	447.5	445	298.3	298.9	296
$D/10^4$ cm^2 s^{-1}		62.0	67[a]		0.197	0.15[b]
τ/ps	150.3	306.3	213	5.5	12.5	18.7
Z_{col}/ps^{-1}		1.02	0.341		42.90	104

[a]Reference 2.
[b]Reference 53.

C. Local heating effects

First theoretical models of collisional energy transfer from ''hot'' azulene in the liquid phase were based on the assumption that energy transfer between azulene and the collision shell could be described within the IBC model, whereas energy transport within the solvent occurred by heat conduction.[12] According to these calculations, energy flowing from solute to solvent rapidly heats the immediate surrounding of azulene which then has a strong impact on the energy-transfer rates and the time scale of the cooling process.

We tried to follow these ideas in our model by monitoring the time dependence of the normalized kinetic energy distribution ρ_{kin}, where ρ_{kin} is defined as the sum of the kinetic energy over all CO_2 molecules i at a distance $r+\delta r$ normalized with respect to the average kinetic energy in the system and the number density ρ:

$$\rho_{kin}=\frac{\Sigma_i E^i_{kin}}{4\pi r^2 \delta r \rho \langle E_{kin}\rangle} \tag{9}$$

with $\delta r = 0.1$ Å.

Due to the fact that at equilibrium the average temperature of a CO_2 molecule is independent of its position with respect to the azulene molecule, $\rho_{kin}(r)$ shows the same structure as $g(r)_{com\text{-}com}$, a maximum in $g(r)$ leads to a maximum in $\rho_{kin}(r)$ because of the increased number density at this distance.

For a discussion of the local heating assumption we evaluated ρ_{kin} at high pressure for the nonequilibrium case as a function of time. We found that these energy distributions maintain their basic spatial structure during the cooling process showing no indication of any systematic heating or cooling at certain times or distances.

As the spatial distributions show, the inner solvation shells exhibit a high degree of anisotropy which is not included in the radial energy distribution. Therefore we monitored the time evolution of the kinetic energy within three inner shells during energy transfer (Fig. 4). As in the case of ρ_{kin}, also the average kinetic energy within all three shells, in spite of statistical fluctuations, which decrease with an increasing level of probability due to an increasing number of solvent molecules occupying shells with high probability in average, remains constant during the cooling of azulene. This result is in agreement with calculations by Schwarzer *et al.*[2] which ruled out heat conduction as a rate limiting step in energy transfer from highly excited azulene molecules.

D. Collision frequency scaling of energy transfer rates

One of the crucial questions in the discussion of the IBC model for liquids is the precise definition of a collision. There are several possible definitions discussed in the literature.[20,44–46] Here we follow an idea of Ohmine,[47] defining an encounter to be a collision when the short-range repulsive potential between CO_2 and azulene $\Phi^{short}_{azul\text{-}CO_2}=\Sigma_\alpha^{N_\alpha}\Sigma_\beta^{N_\beta}[A_{\alpha\beta}/r^{12}_{\alpha\beta}-B_{\alpha\beta}/r^6_{\alpha\beta}]$ exceeds a certain critical value V_{lim}, which we chose as 0 kcal mol^{-1}.

In Fig. 5 we summarize statistical data on collisions, defined by this approach. According to our results at 3.2 and 250 MPa, collisions occur at an average energy of $\sim$0.5 kcal mol^{-1} and an average distance of $\sim$5.5 Å. A collision at 3.2 MPa lasts about 22.8 fs, and at the higher pressure is only slightly shorter (21.4 fs). From these results, we draw the conclusion that, within our model, the collision mechanism itself is pressure independent, as was suggested earlier.[36] Collision frequencies Z calculated on the basis of this energetic collision criterion for high- and low-pressure range around 43 and 11 ps^{-1}, respectively.

Another possibility to estimate collision rates was proposed by Einwohner and Alder[44,36,48] on the basis of geometric considerations. This geometric collision frequency is defined by the flux through a spherical shell around azulene at a certain distance as

$$Z(r)=\pi r^2 \frac{N}{V}\langle c_{rel}\rangle g(r), \tag{10}$$

with $\langle c_{rel}\rangle$ being the average relative velocity of a CO_2 molecule approaching the azulene and $g(r)$ being the COM-COM pair distribution function. As discussed by Darid and Cukier[48] there is no rigorous basis for choosing the distance r_{col} where a collision is defined to take place, because a small r_{col} leads to poor averaging and a large r_{col} to an exclusion of many-body effects. For the case of a Lennard–Jones fluid, it

was proposed to set r_{col} to σ_{LJ}.[45] To facilitate comparison with the values derived by the energy criterion, we chose r_{col} to be the shortest distance where $g(r)$ equals unity, i.e., the point where the average potential should be zero. Therefore r_{col} is no longer a fixed distance but a pressure dependent variable (Fig. 6). Using this definition, we calculated values for Z of $0.161\ \mathrm{ps}^{-1}$ ($r_{\mathrm{col}}=4.875$ Å) and $4.622\ \mathrm{ps}^{-1}$ ($r_{\mathrm{col}}=5.332$ Å) at 3.2 and 250 MPa, respectively (cf. Fig. 6), i.e., the rates are one order of magnitude smaller than those derived from the energetic criterion. Assuming the validity of an IBC energy-transfer model, from the simulated energy decay rates one would expect the ratio $Z(250\ \mathrm{MPa})/Z(3.2\ \mathrm{MPa})$ to be ~ 25 for both model a and b. With 37.75 and 28.62, similar ratios are obtained from the energetic and geometric definition of a collision, respectively. Thus as far as scaling with collision frequency is concerned, there seem to be no signs of a breakdown of the IBC assumption considering the uncertainty in defining what a collision is under the given conditions.

For both definitions the calculated collision frequencies Z deviate strongly from the $Z_D(P_i)$ values[2] [$Z_D(3.2\ \mathrm{MPa})=0.341\ \mathrm{ps}^{-1}$, $Z_D(308\ \mathrm{MPa})=104\ \mathrm{ps}^{-1}$] predicted on the basis of the Lennard–Jones frequency Z_{LJ} and semiempirical scaling with the solvent self-diffusion coefficient[6,49–51] (Table VIII):

$$Z_D(p_2)=\frac{Z_{\mathrm{LJ}}(p_1)D(p_1)}{D(p_2)}, \tag{11}$$

where $D(p_i)$ is the measured diffusion coefficient at the respective pressure. The large discrepancy could indicate that energy transfer occurs on a time scale shorter than or comparable with that required for attaining the regime of a stationary diffusion coefficient.

IV. CONCLUSION

The results for vibrational cooling rates of azulene in CO_2 from molecular-dynamics trajectories are qualitatively consistent with experimental measurements under similar conditions. In accordance with the binary collision model, it is found that cooling rates are strongly density dependent, while the functional form of the energy loss curves is approximately monoexponential and independent of the thermodynamic state of the system.

A structural analysis, carried out at high pressure, reveals a well-defined shell structure of the solvent. Nevertheless the spatial analysis gives no indication that the local anisotropy of the solvent shell influences the collision mechanism. In particular, local heating effects of any kind do not appear in our simulations.

ACKNOWLEDGMENTS

The authors thank Professor Jürgen Troe for continued support and encouragement. C.H. is grateful to the Fonds der Chemischen Industrie for financial support.

[1] C. B. Harris, D. E. Smith, and D. J. Russell, Chem. Rev. **90**, 481 (1990).
[2] D. Schwarzer, J. Troe, M. Votsmeier, and M. Zerezke, J. Chem. Phys. **105**, 3121 (1996).
[3] D. Schwarzer, J. Troe, and M. Zerezke, J. Chem. Phys. **107**, 8380 (1997).
[4] D. Schwarzer, J. Troe, and M. Zerezke, J. Phys. Chem. A (to be published).
[5] K. F. Herzfeld and T. A. Litovitz, *Absorption and Dispersion of Ultrasonic Waves* (Academic, New York, 1959).
[6] R. Zwanzig, J. Chem. Phys. **34**, 1931 (1961).
[7] D. W. Oxtoby, Adv. Chem. Phys. **47**, 487 (1981).
[8] P. S. Darid and R. I. Cukier, J. Chem. Phys. **86**, 2264 (1987).
[9] J. Benzler, S. Linkersdörfer, and K. Luther, J. Chem. Phys. **106**, 4992 (1997).
[10] F. Wondrazek, A. Seilmeier, and W. Kaiser, Chem. Phys. Lett. **104**, 121 (1984).
[11] A. Seilmeier, P. O. J. Scherer, and W. Kaiser, Chem. Phys. Lett. **105**, 140 (1984).
[12] U. Sukowski, A. Seilmeier, T. Elsaesser, and S. F. Fischer, J. Chem. Phys. **93**, 4094 (1990).
[13] K. E. Schultz, D. J. Russel, and C. B. Harris, J. Chem. Phys. **97**, 5431 (1992).
[14] T. Lenzer, K. Luther, J. Troe, R. G. Gilbert, and K. F. Lim, J. Chem. Phys. **103**, 627 (1995).
[15] R. G. Gilbert, Aust. J. Chem. **48**, 1787 (1995).
[16] T. Lenzer and K. Luther, J. Chem. Phys. **109**, 3391 (1996).
[17] L. Ming, J. Davidsson, and S. Nordholm, J. Chem. Phys. **104**, 9001 (1996).
[18] J. K. Brown and C. B. Harris, J. Chem. Phys. **89**, 6687 (1988).
[19] P. Moore, A. Tokmakoff, T. Keyes, and M. D. Fayer, J. Chem. Phys. **103**, 3325 (1995).
[20] Q. Liu, C. Wan, and A. H. Zewail, J. Phys. Chem. **100**, 18666 (1996).
[21] Q. Liu, C. Wan, and A. H. Zewail, J. Chem. Phys. **105**, 5294 (1996).
[22] M. P. Allen and D. J. Tildesley, *Computer Simulation of Liquids* (Oxford University Press, Oxford, 1987).
[23] O. Gebhardt, Acta Chem. Scand. **27**, 1725 (1973).
[24] Molecular Simulations Incorporated, QUANTA 4.0., 1994.
[25] S.-B. Zhu and G. W. Robinson, Comput. Phys. Commun. **52**, 317 (1989).
[26] I. I. Fedchenia and J. Schroeder, J. Chem. Phys. **106**, 7749 (1997).
[27] L. M. Nxumalo and T. A. Ford, J. Mol. Struct. **145**, 153 (1994).
[28] H. J. Böhme, R. Ahlrichs, P. Scharf, and H. Schiffer, J. Chem. Phys. **81**, 1389 (1984).
[29] H. J. Böhme, C. Meissner, and R. Ahlrichs, Mol. Phys. **53**, 651 (1984).
[30] H. J. Tobler, A. Bauer, and H. H. Günthard, J. Mol. Spectrosc. **18**, 239 (1965).
[31] A. G. Anderson and B. M. Steckler, J. Am. Chem. Soc. **81**, 4941 (1959).
[32] M. W. Schmidt, K. K. Baldirge, J. A. Boatz, S. T. Elbert, M. S. Gordon, J. H. Jensen, S. Koseki, N. Matsunaga, K. A. Nguyen, S. J. Su, T. L. Windus, M. Dupius, and J. A. Montgomery, J. Comput. Chem. **14**, 1347 (1993).
[33] Havard University, CHARMM 24.b1., 1995.
[34] K. Bolton and S. Nordholm, Chem. Phys. **203**, 101 (1996).
[35] P. K. Davis and I. Oppenheim, J. Chem. Phys. **56**, 86 (1972).
[36] P. K. Davis and I. Oppenheim, J. Chem. Phys. **57**, 505 (1972).
[37] H. Tanaka and I. Ohmine, J. Chem. Phys. **87**, 6128 (1987).
[38] R. Ishii, S. Okazaki, and I. Okada, J. Chem. Phys. **105**, 7011 (1996).
[39] P. G. Debenedetti, Chem. Eng. Sci. **42**, 2203 (1987).
[40] I. B. Petsche and P. G. Debenedetti, J. Chem. Phys. **91**, 7075 (1989).
[41] H. Inomata, S. Saito, and P. G. Debenedetti, Fluid Phase Equilibria **116**, 282 (1996).
[42] I. M. Svischev and P. G. Kusalik, J. Chem. Phys. **99**, 3049 (1993).
[43] I. M. Svischev and P. G. Kusalik, J. Chem. Phys. **100**, 5165 (1994).
[44] T. Einwohner and B. J. Alder, J. Chem. Phys. **49**, 1459 (1968).
[45] P. K. Davis, J. Chem. Phys. **57**, 517 (1972).
[46] J. K. Broen, D. J. Russell, and C. B. Harris, Rev. Phys. Appl. **22**, 1787 (1988).
[47] I. Ohmine, J. Chem. Phys. **85**, 3342 (1986).
[48] P. S. Darid and R. I. Cukier, J. Chem. Phys. **7**, 4145 (1988).
[49] B. Otto, J. Schroeder, and J. Troe, J. Chem. Phys. **81**, 202 (1984).
[50] H. Hippler, V. Schubert, and J. Troe, J. Chem. Phys. **81**, 3931 (1984).
[51] G. Maneke, J. Schroeder, J. Troe, and F. Voss, Ber. Bunsenges. Phys. Chem. **89**, 896 (1985).
[52] R. S. Chao and R. K. Khanna, Spectrochim. Acta A **33**, 53 (1977).
[53] V. V. Altunin, Tr. Mosk. Energ. In-ta. **424**, 24 (1979).